Mobile bound states of Rydberg excitations in a lattice

Fabian Letscher
Department of Physics and Research Center OPTIMAS, University of Kaiserslautern, D-67663 Kaiserslautern, Germany and Graduate School Materials Science in Mainz, Gottlieb-Daimler-Strasse 47, D-67663 Kaiserslautern, Germany

David Petrosyan
Institute of Electronic Structure and Laser, FORTH, GR-71110 Heraklion, Crete, Greece

(Received 21 December 2017; published 16 April 2018)

Spin-lattice models play a central role in the studies of quantum magnetism and nonequilibrium dynamics of spin excitations——magnons. We show that a spin lattice with strong nearest-neighbor interactions and tunable long-range hopping of excitations can be realized by a regular array of laser-driven atoms, with an excited Rydberg state representing the spin-up state and a Rydberg-dressed ground state corresponding to the spin-down state. We find exotic interaction-bound states of magnons that propagate in the lattice via the combination of resonant two-site hopping and nonresonant second-order hopping processes. Arrays of trapped Rydberg-dressed atoms can thus serve as a flexible platform to simulate and study fundamental few-body dynamics in spin lattices.

DOI: 10.1103/PhysRevA.97.043415

I. INTRODUCTION

Interacting many-body quantum systems are notoriously difficult to simulate on classical computers, due to the exponentially large Hilbert space and quantum correlations between the constituents. It was therefore suggested to simulate quantum physics with quantum computers [1], or universal quantum simulators consisting of spin lattices with tunable interactions between the spins [2]. Dynamically controlled spin lattices can realize digital and analog quantum simulations. Quantum field theories not amenable to perturbative treatments are often discretized and mapped onto the lattice models for numerical calculations. Spin lattices are fundamental to the studies of many solid-state systems, where the competition between the interaction and kinetic energies determines such phenomena as magnetism and superconductivity.

Realizing tunable spin lattices in the quantum regime is challenging. Several systems are being explored to this end, including trapped ions [3,4], superconducting circuits [5,6], quantum dots [7], and other solid-state systems. Cold atoms in optical lattice potentials are accurately described by the Hubbard model, representing perhaps the most versatile and scalable platform to realize various lattice models [8]. The Hubbard model for two-state fermions or strongly interacting bosons at half filling can implement the lattice spin-1/2 model [9,10]. The spin-exchange interaction then stems from the second-order tunneling (superexchange) process [11,12] and the interspin Ising interaction can exist for atoms or molecules with static magnetic or electric dipole moments [13,14]. These interactions are, however, weak (tens of hertz or less), which makes the system vulnerable to thermal effects even at ultralow temperatures of nanokelvins [15–17].

Here we propose a practical realization of a tunable spin lattice XXZ model with an array of trapped atoms [18,19]. The atomic ground state dressed by a nonresonant laser with a Rydberg state [20–23] represents the spin-down state, while another Rydberg state corresponds to the spin-up state (see Fig. 1). Controllable spin-exchange interactions are then mediated by the dressing laser and resonant dipole-dipole exchange interaction (scaling with distance r as $1/r^3$) between the atoms on the Rydberg transition. The van der Waals interactions between the excited-state atoms (scaling as $1/r^6$) serve as Ising-type interaction between the spins [24–28]. Due to long lifetimes of the Rydberg states and large energy scales of their interactions, this system is essentially at zero temperature. This permits observation of coherent quantum dynamics of spin excitations—magnons.

We study the dynamics of magnons in the spin-lattice with long-range spin-excitation hopping and nearest-neighbor interactions. Apart from scattering states, we find exotic interaction-bound states of magnons [29]. The bound pairs of magnons can propagate in the lattice via resonant two-site spin exchange and nonresonant second-order exchange interactions [see Fig. 1(a)]. We note that the spin-lattice XXZ model can be mapped onto the extended Hubbard model with spinless fermions or hard-core bosons: In the extended Hubbard model with low filling, particle tunneling from site to site and the attractive or repulsive interactions between the particles at the neighboring sites correspond, in the spin-lattice model, to the excitation hopping via spin exchange and to the Ising interspin interaction, respectively. The bound states of magnons are then equivalent to interaction bound states of particles in the (extended) Hubbard model [29,30]. But our solution goes beyond the bound-state solutions of the Hubbard model [31–37] and it can be easily generalized to arbitrary-range hopping and interactions. We find that longer-range hopping of individual magnons leads to the increased, and tunable, mobility of the bound pairs.

II. INTERACTING SPIN EXCITATIONS IN A LATTICE

We consider a spin-lattice model described by the Hamiltonian ($\hbar = 1$)

$$\mathcal{H} = \sum_{i<j} J_{ij}(\hat{\sigma}_i^+\hat{\sigma}_j^- + \hat{\sigma}_i^-\hat{\sigma}_j^+) + \sum_{i<j} U_{ij}\hat{n}_i\hat{n}_j, \qquad (1)$$

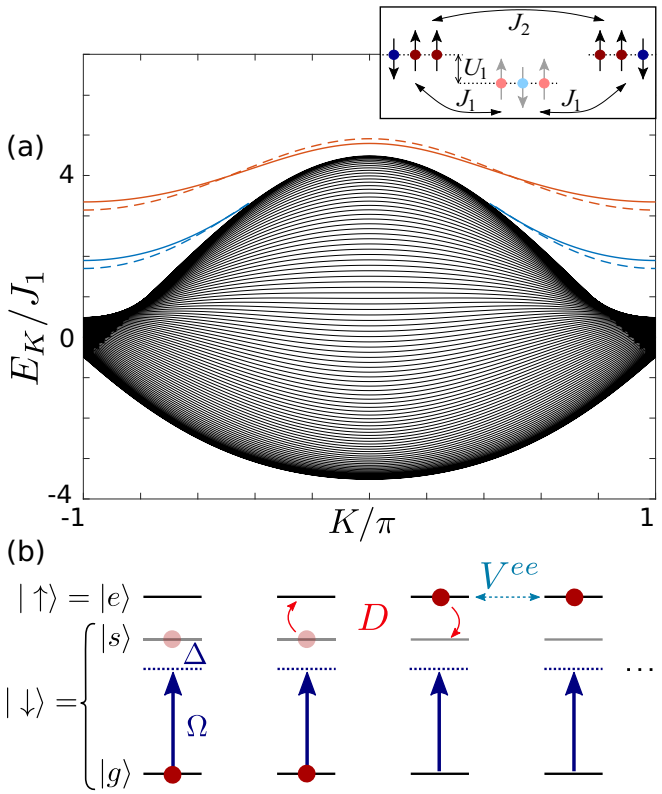

FIG. 1. (a) Spectrum of two spin (Rydberg) excitations in a lattice versus the center-of-mass quasimomentum K. The scattering states form a continuum spectrum (black) [Eq. (7)]. The bound states for strong (red lines) and weak (blue lines) repulsive interactions are obtained from the spin-lattice Hamiltonian (dashed lines) [Eq. (9)] and from exact diagonalization of the Hamiltonian for the system sketched in (b) (solid lines). In the simulations, we used a lattice of size $L = 100$ and periodic boundary conditions, with the spin model parameters $J_2/J_1 = 1/8, U_1/J_1 = 3.4, 1.9$ for the red and blue dashed lines, respectively. The inset illustrates the motion of the bound pair via resonant two-site hopping J_2 and second-order hopping J_1^2/U_1. (b) Level scheme of atoms to realize a spin-lattice model. Atoms in Rydberg states $|e\rangle$ and $|s\rangle$ undergo dipole-dipole exchange interaction $|es\rangle \to |se\rangle$ with rate D. The atomic ground state $|g\rangle$ is dressed with the Rydberg state $|s\rangle$ by a nonresonant laser with Rabi frequency Ω and detuning $\Delta \gg \Omega$. The spin-up and spin-down states correspond to $|\uparrow\rangle = |e\rangle$ and $|\downarrow\rangle \simeq |g\rangle + \frac{\Omega}{\Delta}|s\rangle$. Interactions V^{ee} between the atoms in state $|e\rangle$ lead to formation of mobile bound states of Rydberg excitations. The parameters in numerical simulations shown in (a) correspond to $\Delta/\Omega = 10$, $D_1/\Omega = 1$, $V_1^{es}/\Omega = -0.125$, and $V_1^{ee}/\Omega = 0.03, 0.015$ for the red and blue solid lines, respectively.

where $\hat{\sigma}_i^+ = |\uparrow\rangle_i\langle\downarrow|$ and $\hat{\sigma}_i^- = |\downarrow\rangle_i\langle\uparrow|$ are the raising and lowering operators for the spin at position i, and $\hat{n}_i \equiv \hat{\sigma}_i^+\hat{\sigma}_i^- = |\uparrow\rangle_i\langle\uparrow|$ is the projector onto the spin-up state. In Eq. (1), the first term is responsible for the spin transport via the exchange interaction J_{ij}, while the second term describes the interaction between the spins in state $|\uparrow\rangle$ with strength U_{ij}. Both J_{ij} and U_{ij} have finite range and depend only on the distance $r = |i - j|$ between the spins at positions i and j.

A. Single magnon

Hamiltonian (1) preserves the number of spin excitations. For a single excitation, the interaction does not play a role, and the Hamiltonian reduces to

$$\mathcal{H}_J^{(1)} = \sum_{x=1}^{L}\sum_{d\geqslant 1} J_d(|x\rangle\langle x+d| + |x\rangle\langle x-d|), \tag{2}$$

where $|x\rangle \equiv \hat{\sigma}_x^+|\downarrow_1\downarrow_2\cdots\downarrow_L\rangle$ denotes the state with the spin up at position x in a lattice of $L \gg 1$ spins (we assume periodic boundary conditions), and $d = 1,2,\ldots$ is the range of the exchange interaction. The transformation $|x\rangle = \frac{1}{\sqrt{L}}\sum_q e^{iqx}|q\rangle$ diagonalizes the Hamiltonian,

$$\mathcal{H}_J^{(1)} = \sum_q |q\rangle\langle q|E_q^{(1)}, \tag{3}$$

which indicates that the plane waves $|q\rangle = \frac{1}{\sqrt{L}}\sum_x e^{iqx}|x\rangle$ with the lattice quasimomenta $q = \frac{2\pi\nu}{L}$ $(\nu = -\frac{L-1}{2},\ldots,\frac{L-1}{2})$ are the eigenstates of $\mathcal{H}_J^{(1)}$ with the eigenenergies $E_q^{(1)} = \sum_{d\geqslant 1} 2J_d\cos(qd)$.

B. Two magnons

Consider now two spin excitations. We denote by $|x,y\rangle$ the state with one spin up at position x and the second spin up at $y > x$. The total Hamiltonian $\mathcal{H}^{(2)} = \mathcal{H}_J^{(2)} + \mathcal{H}_U^{(2)}$ consists of the transport and interaction terms:

$$\begin{aligned}\mathcal{H}_J^{(2)} = \sum_{x<y}\Bigg[&\sum_d J_d(|x,y\rangle\langle x-d,y| + |x,y\rangle\langle x,y+d|)\\ &+ \sum_{d<y-x} J_d(|x,y\rangle\langle x+d,y| + |x,y\rangle\langle x,y-d|)\\ &+ \sum_{d>y-x} J_d(|x,y\rangle\langle y,x+d| + |x,y\rangle\langle y-d,x|)\Bigg],\end{aligned} \tag{4}$$

$$\mathcal{H}_U^{(2)} = \sum_{x<y} U_{xy}|x,y\rangle\langle x,y|. \tag{5}$$

We introduce the center of mass $R \equiv (x+y)/2$ and relative $r \equiv y - x$ coordinates. Making the transformation $|R\rangle = \frac{1}{\sqrt{\tilde{L}}}\sum_K e^{iKR}|K\rangle$ $(\tilde{L} = 2L - 3)$, we obtain the total Hamiltonian $\mathcal{H}^{(2)}$ that is diagonal in the basis $|K\rangle$ of the center-of-mass quasimomentum $K = \frac{2\pi\nu}{\tilde{L}}$: $\mathcal{H}^{(2)} = \sum_K |K\rangle\langle K| \otimes \mathcal{H}_K$, where

$$\begin{aligned}\mathcal{H}_K = \sum_r\Bigg[&\sum_d J_{d,K}|r\rangle\langle r+d| + \sum_{d<r} J_{d,K}|r\rangle\langle r-d|\\ &+ \sum_{d>r} J_{d,K}|r\rangle\langle d-r| + U_r|r\rangle\langle r|\Bigg],\end{aligned} \tag{6}$$

with $J_{d,K} \equiv 2J_d\cos(Kd/2)$ (see Appendix A). The two-body wave function can be cast as $|\Psi(x,y)\rangle = \frac{1}{\sqrt{\tilde{L}}}\sum_K e^{iKR}|K\rangle \otimes \sum_{r\geqslant 1}\psi_K(r)|r\rangle$, where the relative coordinate wave function $\psi_K(r)$ depends on the quasimomentum K as a parameter via the effective hopping rates $J_{d,K}$ in $\mathcal{H}_K$. There are two kinds of solutions of the eigenvalue problem $\mathcal{H}_K|\psi_K\rangle = E_K|\psi_K\rangle$ for $|\psi_K\rangle = \sum_{r\geqslant 1}\psi_K(r)|r\rangle$, corresponding to scattering states of asymptotically free magnons and to the interaction-bound states.

1. Scattering states

The wave function for the scattering states has the standard form containing the incoming and scattered plane waves $\psi_{K,k}(r > d_U) = e^{ikr} + e^{-2i\delta_{K,k}}e^{-ikr}$, where d_U is the (finite) range of the interaction potential U_r, and the phase shift $\delta_{K,k}$ depends on U_r. The energies of the scattering states are simply given by the sum of energies of two free magnons,

$$E^{(s)}_{K,k} = E^{(1)}_{q_1} + E^{(1)}_{q_2} = \sum_d 2J_{d,K}\cos(kd), \tag{7}$$

where $K = q_1 + q_2$ and $k = (q_1 - q_2)/2$ are the center-of-mass and relative quasimomenta. In Fig. 1(a) we show the spectrum of the scattering states, assuming the range of the spin-exchange interaction $d_J = 2$ with $J_1 > J_2$, while $J_{d\geqslant 3} = 0$. Note that due to the longer-range hopping J_2, the spectrum at $K = \pm\pi$ does not reduce to a single point $E^{(s)} = 0$ as in Refs. [33,34] but has a finite width $E^{(s)}_{K=\pi,k} \in [-4J_2, 4J_2]$ (see also Refs. [31,37]).

2. Bound states

The bound-state solutions correspond to a normalizable relative coordinate wave function, $\sum_r |\psi_K(r)|^2 = 1$. We assume nearest-neighbor interaction, $U_1 \neq 0$ and $U_{r>1} = 0$ in Eq. (6). We set $\psi_K(0) = 0$ and $\psi_K(1) = c$, with c some constant, and make the ansatz

$$\psi_K(r) = \alpha_K\psi_K(r-1) + \beta_K\psi_K(r-2). \tag{8}$$

The physical intuition behind this recurrence relation is that every (discrete) position r can be reached from positions $r-1$ and $r-2$ with the amplitudes $\alpha_K \propto J_1$ and $\beta_K \propto J_2$. We then obtain (see Appendix A) $\alpha_K = \frac{J_{1,K}}{U_1}$, $\beta_K = \frac{J_{2,K}}{U_1 + J_{2,K}}$, and the energy of the bound state,

$$E^{(b)}_K = 2J_{2,K} + \frac{J^2_{1,K}}{U_1} + \frac{J^2_{1,K}J_{2,K}}{U^2_1} + \frac{U^2_1}{U_1 + J_{2,K}}. \tag{9}$$

The first term on the right-hand side of this equation does not depend on the interaction U_1 and it describes two-site resonant hopping of the excitation over the other excitation, $|x-1,x\rangle \leftrightarrow |x,x+1\rangle$, with rate $\propto J_2$. This process is resonant because the relative distance $r = 1$, and thereby the interaction energy, is conserved during this two-excitation "somersault." The second and third terms are contributions from the second-order ($\propto J^2_1/U_1$) and third-order ($\propto J^2_1 J_2/U^2_1$) hopping processes. The last term is the energy shift due to interaction U_1.

The above solution is valid under the conditions that bound-state wave function is normalizable. Inserting $\psi_K(r) \propto \lambda^r$ into Eq. (8), we obtain that the wave function exponentially decays with distance r, and therefore is normalizable, when $\frac{1}{2}|\alpha_K \pm \sqrt{\alpha^2_K + 4\beta^2_K}| < 1$ (see Appendix A). This condition also means that the energy of the bound state, $E^{(b)}_K$, in Eq. (9) is outside the energies of the scattering continuum, $E^{(s)}_{K,k}$, in Eq. (7). In Fig. 2(a) we show the values of α_K and β_K, forming a triangular region, for which there exists an exponentially localized bound state. With only nearest-neighbor hopping ($J_2 = 0$), we recover the condition $|\alpha_K| < 1$ of Refs. [33,34]. For a given set of parameters J_1, J_2, U_1, the bound state may not exist for all values of the center-of-mass quasimomentum K, since both α_K and β_K depend on K. In general, the closer is the point (α_K, β_K) to the boundary of the shaded region in Fig. 2(a), the less localized is the bound-state wave function, as we illustrate in Fig. 2(b). In Fig. 3 we show the diagrams of J_2/J_1 and U_1/J_1 versus K for the existence of the bound states.

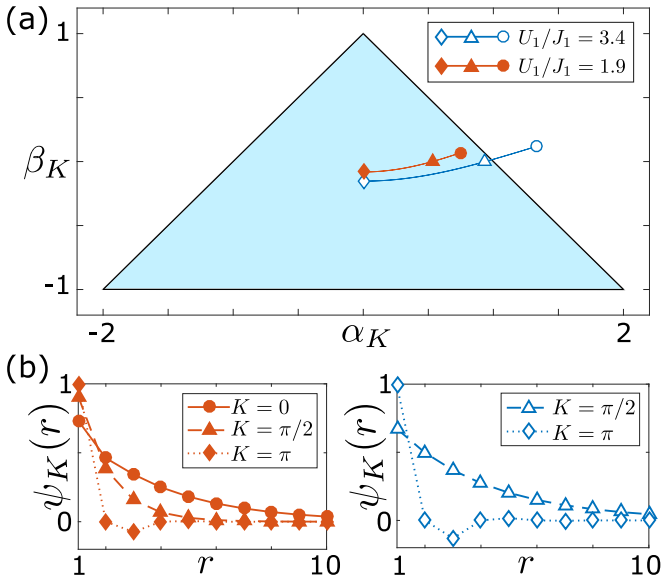

FIG. 2. (a) Diagram of values of α_K and β_K for the existence of bound states (light blue shaded region). (b) Wave function $\psi_K(r)$ versus the relative distance r for several values of the center-of-mass quasimomentum K. The parameters are the same as in Fig. 1, with $U_1/J_1 = 3.4$ [left graph and red line in (a)], and $U_1/J_1 = 1.9$ [right graph and blue line in (a)], where the bound state does not exist in the vicinity of $K = 0$.

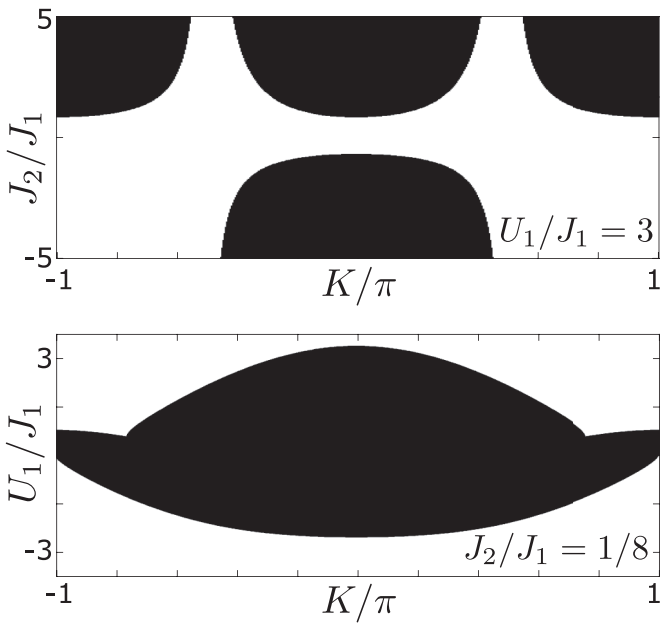

FIG. 3. Diagram of values of J_2/J_1, for fixed $U_1 = 3J_1$ (upper panel), and U_1/J_1, for fixed $J_2 = J_1/8$ (lower panel), versus K, for the existence (white regions) and absence (black regions) of the bound states.

Note that both attractive ($U_1 < 0$) and repulsive ($U_1 > 0$) interactions can sustain bound states. Clearly, for certain sets of parameters, the bound states do not exist at all, or exist only within a certain interval of values of K.

III. RYDBERG DRESSED ATOMS IN A LATTICE

The spin-lattice model of Eq. (1) might be realized with a regular array of atoms in Rydberg states $|s\rangle$ and $|e\rangle$. One or more atoms could be excited to state $|e\rangle = |\uparrow\rangle$ while all the remaining atoms are prepared in state $|s\rangle = |\downarrow\rangle$. Assuming the transition $|s\rangle \leftrightarrow |e\rangle$ is dipole allowed, resonant dipole-dipole interaction between the atoms at lattice positions i and j would lead to transfer of excitations via the exchange interaction $|es\rangle \leftrightarrow |se\rangle$ with rate $D_{ij} = \frac{C_3/a^3}{|i-j|^3}$, where C_3 is the interaction coefficient and a is the lattice constant [38–40]. Atoms in the Rydberg states also interact via the van der Waals interactions $V_{ij}^{\mu\nu} = \frac{C_6^{\mu\nu}/a^6}{|i-j|^6}$, which would map onto the interactions U_{ij} between the spin excitations [24–28], provided V_{ij}^{ee} differs from the interaction V_{ij}^{es} between the $|e\rangle$ and $|s\rangle$ state atoms.

Typically, however, the resonant dipole-dipole interaction D is orders of magnitude stronger than the van der Waals interactions V, since the latter originate from nonresonant dipole-dipole interactions, $V \sim D^2/\delta\omega$, with large Förster defects, $\delta\omega \gg D$ [41]. Small interactions $V \ll D$ will preclude the interplay between the spin transport and spin-spin interactions. In principle, one could explore the angular dependence of the dipole-dipole and van der Waals interactions [42] to tune the relative strengths of D and V, which, however, would be very sensitive to atomic position uncertainties. Moreover, if all the atoms are prepared in the Rydberg state $|s\rangle$, the motion of the untrapped atoms and their decay will strongly affect the system on the timescale of the interaction. To mitigate these problems, we propose to dress trapped ground-state atoms with the Rydberg state $|s\rangle$. The dressing laser would then mediate hopping of the Rydberg excitation $|e\rangle$ to nearby atoms in the dressed ground state with rates J_d which can be made comparable to, or even weaker than, the effective interaction U_r between the excitations. Rydberg dressing of ground-state atoms [20–23,43–45] is a versatile tool for tuning interatomic interactions to simulate various lattice models [46–51].

A. Parameters of the effective lattice Hamiltonian

We consider an array of single atoms with the level scheme shown in Fig. 1(b). The ground state $|g\rangle$ of each atom is coupled to the Rydberg state $|s\rangle$ by a spatially uniform laser with Rabi frequency Ω and detuning $\Delta = \omega_{sg} - \omega \gg |\Omega|$. The corresponding Hamiltonian for the atoms is

$$\mathcal{H}_{\rm at} = \sum_j \left[\Delta\hat{\sigma}_j^{ss} - \left(\Omega\hat{\sigma}_j^{gs} + \text{H.c.}\right)\right] + \sum_{i<j} D_{ij}\left(\hat{\sigma}_i^{es}\hat{\sigma}_j^{se} + \text{H.c.}\right) + \sum_{i<j}\left(V_{ij}^{ee}\hat{\sigma}_i^{ee}\hat{\sigma}_j^{ee} + V_{ij}^{ss}\hat{\sigma}_i^{ss}\hat{\sigma}_j^{ss} + V_{ij}^{es}\hat{\sigma}_i^{ee}\hat{\sigma}_j^{ss}\right), \quad (10)$$

where $\hat{\sigma}_j^{\mu\nu} = |\mu\rangle_j\langle\nu|$ are the atomic operators. We assume that Δ is much larger than the resonant dipole-dipole interactions D_d between the $|s\rangle$ and $|e\rangle$ state atoms separated by $d = 1,2,\ldots$ lattice sites. The van der Waals interactions $V_r^{\mu\nu}$ are assumed to be still weaker, so the hierarchy of the energy scales is $\Delta \gg \Omega, D_d \gtrsim V_r^{ee}, V_r^{es}, V_r^{ss}$.

The laser instills a small admixture $\frac{\Omega}{\Delta}|s\rangle$ of the Rydberg state to the ground state $|g\rangle$ (see Appendix B). We then identify the dressed ground state with the spin-down state, $|\downarrow\rangle \simeq |g\rangle + \frac{\Omega}{\Delta}|s\rangle$, while the spin-up state is $|\uparrow\rangle = |e\rangle$. Neglecting the interactions $\sim\frac{|\Omega|^4}{\Delta^4}V_r^{ss}$ between the dressed ground-state atoms, we adiabatically eliminate the nonresonant state $|s\rangle$ and obtain effective excitation hopping rates

$$J_d \simeq \frac{|\Omega|^2 D_d}{\Delta^2} \quad (11)$$

between the atoms separated by d lattice sites. Since $D_d \propto d^{-3}$, we can truncate J_d to range $d_J = 2$. More careful considerations show that the hopping rates $J_{1,2}$ for a Rydberg excitation are slightly altered when another Rydberg excitation is in close proximity (see Appendix B). We assume that the lifetime of the Rydberg state $|e\rangle$ is longer than the timescale J_d^{-1} for the system dynamics and neglect dissipation. The number of atoms prepared in state $|e\rangle$ is then conserved. Decay via the nonresonant state $|s\rangle$ is suppressed by the factor of $\frac{|\Omega|^2}{\Delta^2}$.

For the effective interaction potential between the excitations we obtain

$$U_r \simeq V_r^{ee} + 2\frac{|\Omega|^2 D_r^2}{\Delta^3}, \quad (12)$$

where both terms scale with distance as $\propto r^{-6}$. U_r is dominated by the nearest-neighbor van der Waals interaction V_1^{ee} between the atoms in Rydberg states $|e\rangle$. Corrections to the level shift of Rydberg-dressed atoms in the vicinity of the Rydberg excited atom $|e\rangle$ lead to a small contribution to U_r and weak longer-range interaction (see Appendix B). Despite these small variations of $J_d(r)$ and U_r with distance r between Rydberg excitations, the spin-lattice model of Eq. (1) approximates well the properties of interacting Rydberg excitations, including the two-excitation bound states shown in Fig. 1(a).

B. Experimental considerations

The dynamics of Rydberg excitations in a lattice and their bound states can be prepared and observed with the presently available experimental techniques. We envisage a defect-free array of cold atoms confined in a one-dimensional optical lattice potential or a chain of microtraps [18,19]. Using focused laser beams, selected atoms can be resonantly excited from the ground state $|g\rangle$ to the Rydberg state $|e\rangle$, while the dressing laser is turned off, $\Omega = 0$. Next, turning on the dressing laser, $\Omega \neq 0$ will lead to the admixture of the Rydberg state $|s\rangle$ to the ground-state atoms, which will induce the $|e\rangle$ excitation hopping between the atoms due the dipole-dipole exchange interaction. With a proper choice of state $|e\rangle$, we can ensure appropriate interaction strength $U_1 \simeq V^{ee} \gtrsim J_1$, which will result in the formation of tightly bound Rydberg excitations that are still mobile as they propagate with rate $\sim J_2$. Free Rydberg excitations and their scattering states can be discriminated from the interaction-bound states spectroscopically or by the fast and slow dynamics, respectively. Turning off the dressing laser would freeze the dynamics, and individual Rydberg excitations can be detected with high efficiency and single-site resolution [26–28].

To be specific, we consider the atomic parameters similar to those in the recent experiments [39,52,53]. The ground state of Rb atoms $|g\rangle = 5S_{1/2}$ can be dressed with the Rydberg state $|s\rangle = 63P_{1/2}$ by a detuned UV laser with the Rabi frequency $\Omega/(2\pi) \simeq 5$ MHz and detuning $\Delta/(2\pi) \simeq 33$ MHz ($\Omega/\Delta = 0.15$). The excited Rydberg state $|e\rangle = 62D_{3/2}$ can be populated by a two-photon transition from the ground state using laser beams focused onto the desired atoms. With the above Rydberg states $|e\rangle$ and $|s\rangle$, the dipole-dipole coefficient for the exchange interaction $D = C_3/r^3$ is $C_3 = 7950$ MHz μm^3 and the van der Waals coefficient for the interaction $V^{ee} = C_6/r^6$ is $C_6 = 730$ GHz μm^6 [39,52,53]. With the lattice constant $a \simeq 10$ μm, we have $U_1 \simeq 730$ kHz, $J_1 \simeq 180$ kHz, and $J_2 \simeq 22$ kHz. Thus the interaction $U_1 \simeq 4J_1$ will support strongly bound states of Rydberg excitations.

In order to observe coherent dynamics of the Rydberg excitations, timescales for decay and relaxations should be longer than $J_{1,2}^{-1} \simeq 5$–50 μs. In the absence of blackbody radiation, the lifetime of state $|e\rangle$ is $\tau_e \simeq 100$ μs, and the dressing state $|s\rangle$ has a similar lifetime $\tau_s \simeq 135$ μs [54] (but the decay of $|s\rangle$ is suppressed by the factor of $|\Omega|^2/\Delta^2$). A cryogenic setup would suppress the blackbody-radiation-induced transitions to other Rydberg states, which moreover can cause additional strong dephasing of the Rydberg states [55–57]. Next the dressing laser phase fluctuations and Doppler shifts of thermal atoms would result in decoherence of the Rydberg excitation dynamics. Recall that the excitation hopping $J_d \simeq \Omega D_d \Omega^*/\Delta^2$ between two atoms involves absorption (Ω) of the laser photon by the ground-state atom, $|g\rangle \to |s\rangle$, dipole-dipole exchange (D_d) with the Rydberg-state atom, $|se\rangle \to |es\rangle$, and then emission ($\Omega^*$) of the laser photon by the second atom, $|s\rangle \to |g\rangle$. Thus, $J_{1,2}$ are susceptible to dephasing of the ground-to-Rydberg transition, which will necessitate the use of a laser with a narrow linewidth of <10 kHz, and cooling the atoms to $T \sim 10$ nK temperatures to eliminate the effects of Doppler broadening. We note that these or similar requirements also apply to most schemes for coherent quantum gates and simulations with Rydberg atoms [41,58].

The dressed ground-state atoms are tightly confined by the microtraps, but the atoms in the Rydberg state are usually not trapped. During the interaction, the Rydberg-excited atoms experience a repulsive (or attractive, if $C_6 < 0$) force $F = -\partial_r V^{ee}(r) = 6C_6/r^7$, which can result in their displacement Δr from the equilibrium lattice positions. We can estimate the displacement for a pair of atoms at the neighboring lattice sites, $r = a$, as $\Delta r \simeq \frac{F(a)}{2m} t^2$, where m is the atomic mass and $t \simeq J_{1,2}^{-1}$ is the timescale of the interaction. We then obtain $\Delta r = 3$–200 nm, which is still smaller than the typical trap waist $\Delta a \lesssim 1$ μm.

We finally note that similar parameters of the spin-lattice model can be obtained for atoms in optical lattices with a smaller period $a \lesssim 1$ μm and tighter confinement $\Delta a \lesssim 100$ nm by choosing lower-lying Rydberg states $|s\rangle$ and $|e\rangle$. Such states, however, have shorter lifetimes, which necessitates larger hopping rates J_d obtained with stronger dressing lasers. Furthermore, at small interatomic separation, the van der Waals interactions between the untrapped Rydberg-excited atoms will exert stronger force [22,59], which can lead to the displacement of atoms comparable to the lattice spacing. This can be mitigated by using "magic wavelength" optical lattices that simultaneously trap the atoms in both the ground state and the Rydberg state [60].

IV. CONCLUSIONS

We have shown that spin-lattice models with controllable long-range hopping and interactions between the spin excitations can be realized with Rydberg-dressed atoms in a lattice. We have found mobile bound states of spin excitations which are quantum lattice solitons. It would be interesting to consider bound aggregates of more than two magnons which may form mobile clusters that can propagate via a resonant long-range hopping process. In turn, multiple clusters can form a lattice liquid [61,62], while including controllable dephasing and disorder [46,63] may change the transport of (bound) Rydberg excitations from ballistic to diffusive or localized. Hence, this system can be used to simulate and study few- and many-body quantum dynamics in spin lattices.

ACKNOWLEDGMENTS

We thank Michael Fleischhauer and Manuel Valiente for valuable advice and discussions. F.L. is supported by a fellowship through the Excellence Initiative MAINZ (DFG/GSC 266) and by DFG through SFB/TR49. D.P. is supported in part by the EU H2020 FET Proactive project RySQ. We are grateful to the Alexander von Humboldt Foundation for travel support via the Research Group Linkage Programme.

APPENDIX A: DETAILS OF DERIVATION OF THE TWO-EXCITATION WAVE FUNCTION IN A SPIN LATTICE

Consider two spin excitations at positions x and $y > x$ in a lattice of $L \gg 1$ sites. The transport and interaction Hamiltonians are given by Eqs. (4) and (5) in the main text. We introduce the center of mass $R \equiv (x + y)/2$ and relative $r \equiv y - x$ coordinates: $R = 1 + \frac{1}{2}, 2, 2 + \frac{1}{2}, \ldots, L - \frac{1}{2}$ takes $\tilde{L} = 2L - 3$ discrete values, and $r = 1, 2, \ldots, L - 1$ takes $L - 1$ values. In terms of these coordinates, the transport Hamiltonian reads

$$\begin{aligned}\mathcal{H}_J^{(2)} = \sum_{R,r}\Bigg[& \sum_d J_d(|R\rangle\langle R - d/2| \otimes |r\rangle\langle r + d| \\ & + |R\rangle\langle R + d/2| \otimes |r\rangle\langle r + d|) \\ & + \sum_{d<r} J_d(|R\rangle\langle R + d/2| \otimes |r\rangle\langle r - d| \\ & + |R\rangle\langle R - d/2| \otimes |r\rangle\langle r - d|) \\ & + \sum_{d>r} J_d(|R\rangle\langle R + d/2| \otimes |r\rangle\langle d - r| \\ & + |R\rangle\langle R - d/2| \otimes |r\rangle\langle d - r|)\Bigg], \end{aligned} \tag{A1}$$

Similarly to the single excitation case, we can diagonalize the center-of-mass part of $\mathcal{H}_J^{(2)}$ by the transformation $|R\rangle = \frac{1}{\sqrt{\tilde{L}}} \sum_K e^{iKR}|K\rangle$, where $K = \frac{2\pi\nu}{\tilde{L}}$ ($\nu = -\frac{\tilde{L}-1}{2}, \ldots, \frac{\tilde{L}-1}{2}$) is the

center-of-mass quasimomentum:

$$\mathcal{H}_J^{(2)} = \sum_K |K\rangle\langle K| \otimes \sum_r \Big[\sum_d J_{d,K} |r\rangle\langle r+d| + \sum_{d<r} J_{d,K} |r\rangle\langle r-d| + \sum_{d>r} J_{d,K} |r\rangle\langle d-r| \Big], \quad \text{(A2)}$$

where $J_{d,K} \equiv 2J_d \cos(Kd/2)$. The interaction Hamiltonian remains diagonal in these coordinates,

$$\mathcal{H}_U^{(2)} = \sum_K |K\rangle\langle K| \otimes \sum_r U_r |r\rangle\langle r|, \quad \text{(A3)}$$

and the total Hamiltonian can be cast as

$$\mathcal{H}^{(2)} = \mathcal{H}_J^{(2)} + \mathcal{H}_U^{(2)} = \sum_K |K\rangle\langle K| \otimes \mathcal{H}_K.$$

We have thus reduced the two-body problem for

$$|\Psi(x,y)\rangle = \sum_{x<y} \Psi(x,y)|x,y\rangle = \frac{1}{\sqrt{\tilde{L}}} \sum_K e^{iKR} |K\rangle \otimes \sum_{r\geqslant 1} \psi_K(r)|r\rangle \quad \text{(A4)}$$

to a one-body problem for the relative coordinate wave function $\psi_K(r)$, which depends on the center-of-mass quasimomentum K as a parameter via the effective hopping rates $J_{d,K}$ in $\mathcal{H}_K$.

Our aim is to solve the eigenvalue problem

$$\mathcal{H}_K |\psi_K\rangle = E_K |\psi_K\rangle \quad \text{(A5)}$$

for the relative coordinate wave function $|\psi_K\rangle = \sum_{r\geqslant 1} \psi_K(r)|r\rangle$. The scattering solutions are expressed via the plane waves as given in the main text. We present here the details of derivation of the bound solutions corresponding to a normalizable (localized) relative coordinate wave function, $\sum_r |\psi_K(r)|^2 = 1$ [with $\psi_K(r\to\infty)\to 0$].

We assume range $d_U = 1$ (nearest-neighbor) interaction, $U_1 \neq 0$ and $U_{r>1} = 0$ in Eq. (A3), leading to the Hamiltonian

$$\mathcal{H}_K = \sum_{r\geqslant 1} [J_{1,K}(|r\rangle\langle r+1| + |r+1\rangle\langle r|) + J_{2,K}(|r\rangle\langle r+2| + |r+2\rangle\langle r|)] + (U_1 + J_{2,K})|1\rangle\langle 1|. \quad \text{(A6)}$$

This results in the equation

$$J_{1,K}[\psi_K(r+1) + \psi_K(r-1)] + J_{2,K}[\psi_K(r+2) + \psi_K(r-2)] + (U_1 + J_{2,K})\delta_{r,1}\psi_K(r) = E_K \psi_K(r). \quad \text{(A7)}$$

We set $\psi_K(0) = 0$ and $\psi_K(1) = c$, with c some constant to be determined by the normalization. We make an ansatz for the wave function,

$$\psi_K(r) = \alpha_K \psi_K(r-1) + \beta_K \psi_K(r-2). \quad \text{(A8)}$$

The physical meaning of this recurrence relation is that every site r can be reached from the previous two sites $r-1$ and $r-2$ with the amplitudes $\alpha_K \propto J_1$ and $\beta_K \propto J_2$. Starting from position $r = 1$, the wave function at any r can then be written as

$$\psi_K(r) = c \sum_{n=0}^{\lfloor (r-1)/2 \rfloor} \binom{r-1-2n}{n} \alpha_K^{r-1-2n} \beta_K^n, \quad \text{(A9)}$$

where $\lfloor\cdot\rfloor$ is the floor function, and the binomial coefficients count the weights for different paths from site 1 to $r > 1$. For instance, we can reach $|r = 4\rangle$ from $|1\rangle$ by three one-site hoppings $\propto\alpha_K^3$, or by two-site hopping β_K followed by one-site hopping α_K, or vice versa, $\propto\beta_K\alpha_K + \alpha_K\beta_K = 2\alpha_K\beta_K$. Using the ansatz (A9) in Eqs. (A7) for $r = 1,2,3$ we obtain a set of three equations,

$$E_K = (U_1 + J_{2,K}) + J_{1,K}\alpha_K + J_{2,K}(\alpha_K^2 + \beta_K), \quad \text{(A10a)}$$

$$E_K\alpha_K = J_{1,K}(\alpha_K^2 + \beta_K + 1) + J_{2,K}(\alpha_K^3 + 2\alpha_K\beta_K), \quad \text{(A10b)}$$

$$E_K(\alpha_K^2 + \beta_K) = J_{1,K}(\alpha_K + \alpha_K^3 + 2\alpha_K\beta_K) + J_{2,K}(1 + \alpha_K^4 + 3\alpha_K^2\beta_K + \beta_K^2), \quad \text{(A10c)}$$

for the unknowns α_K, β_K, and E_K. Solving these equations, we obtain

$$\alpha_K = \frac{J_{1,K}}{U_1}, \quad \beta_K = \frac{J_{2,K}}{U_1 + J_{2,K}}, \quad \text{(A11)}$$

while the energy of the bound state is

$$E_K^{(\mathrm{b})} = 2J_{2,K} + \frac{J_{1,K}^2}{U_1} + \frac{J_{1,K}^2 J_{2,K}}{U_1^2} + \frac{U_1^2}{U_1 + J_{2,K}}. \quad \text{(A12)}$$

The physical meanings of the various terms of this equation are discussed in the main text.

We finally discuss the conditions of validity of the above solution under which the bound-state wave function is normalizable, $\sum_r |\psi_K(r)|^2 = 1$. Assuming $\psi_K(r) \propto \lambda^r$ and inserting into Eq. (A8), we obtain the quadratic equation $\lambda^2 = \alpha_K\lambda + \beta_K$ with the solutions

$$\lambda_{1,2} = \frac{\alpha_K \pm \sqrt{\alpha_K^2 + 4\beta_K^2}}{2}. \quad \text{(A13)}$$

We can now write the wave function as

$$\psi_K(r) = c_1\lambda_1^r + c_2\lambda_2^r, \quad \text{(A14)}$$

and determine the coefficients $c_{1,2}$ from $\psi_K(0) = 0$ and $\psi_K(1) = c$, leading to $c_2 = -c_1 = \frac{c}{\sqrt{\alpha_K^2+4\beta_K^2}}$. This is of course the same wave function as in Eq. (A9). More important, however, is that we have found that $\psi_K(r) \propto \lambda_{1,2}^r$ exponentially decays with distance r, and therefore is normalizable, when both $|\lambda_{1,2}| = \frac{1}{2}|\alpha_K \pm \sqrt{\alpha_K^2 + 4\beta_K^2}| < 1$.

1. Truncation of interaction range

Our formalism to obtain the bound states of excitations in a lattice can be easily extended to longer-range hopping J_d and interaction U_r. We are, however, mainly concerned with the typical case of resonant dipole-dipole exchange interaction, leading to $J_d \propto 1/d^3$, and van der Waals repulsive or attractive interaction, leading to $U_r \propto 1/r^6$. We have therefore truncated

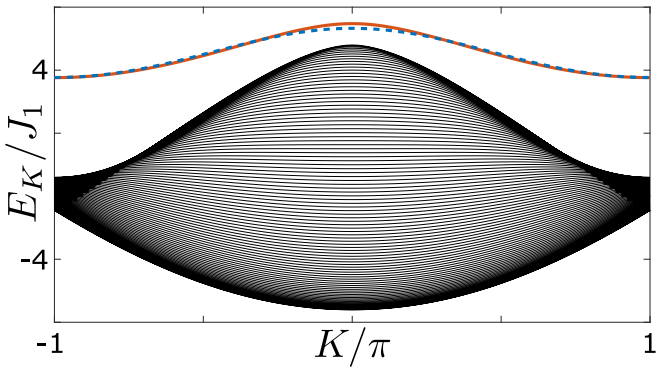

FIG. 4. Scattering (black) and bound-state (red solid line) spectra obtained by exact numerical diagonalization of Hamiltonian with long-range interactions $J_d = J_1/d^3$ and $U_r = U_1/r^6$ ($U_1/J_1 = 4$). The bound-state energy E_K of Eq. (A12) (dashed blue line), obtained with truncated interactions ($d_J = 2$ and $d_U = 1$), is nearly indistinguishable from the exact result.

J_d to range $d_J = 2$ and U_r to range $d_U = 1$. In Fig. 4 we show the spectra for the scattering and bound states obtained without the truncation. This figure clearly demonstrates that the above approximations are well justified for the power-law decay of the strengths of J_d and U_r with distance.

2. Periodic versus open boundary conditions

Our treatment of spin excitations in a lattice assumes periodic boundary conditions, leading to simple analytic and numerical solutions, which also apply to infinitely long lattices. But our results should also hold for a sufficiently long lattice with open boundary conditions. We can define the localization length ζ of the bound-pair wave function via $|\psi_K(r)| \propto e^{-r/\zeta}$, leading to $\zeta \simeq -1/\ln(|\lambda_i|)$, where λ_i is the smaller (in absolute value) root in Eq. (A13). Then, if we require that $L \gg \zeta$, the wave function and energies of the bound pair will not be significantly modified by the boundary conditions in a finite lattice of length L. For a shorter spin lattice, however, one has to exactly diagonalize the system Hamiltonian, and the eigenstates and eigenfunctions will strongly depend on the boundary conditions. In fact, for a short system, $L \sim \zeta$, it may not be possible to clearly distinguish the bound and scattering states. We have checked numerically that, for our parameters, the system size $L > 10$ is sufficient to resolve the bound magnon pairs. We note that lattices with periodic boundary conditions have been realized for atoms in optical tweezers in Ref. [26].

APPENDIX B: DERIVATION OF THE EFFECTIVE EXCITATION HOPPING RATE AND INTERACTION STRENGTH FOR RYDBERG-DRESSED ATOMS IN A LATTICE

Consider an ensemble of atoms in a lattice described by the Hamiltonian of Eq. (10). We take the detuning Δ of the laser field to be much larger than the Rabi frequency Ω as well as the resonant dipole-dipole interactions $D_d = \frac{C_3/a^3}{d^3}$ between the Rydberg-state atoms separated by $d = 1,2,\ldots$ lattice sites. The van der Waals interactions $V_d^{\mu\nu} = \frac{C_6^{\mu\nu}/a^6}{d^6}$ are assumed to be still weaker, $\Delta \gg \Omega, D_d > V_d^{ee}, V_d^{es}, V_d^{ss}$.

1. Rydberg dressing

For a single (isolated) atom, the dipole-dipole and van der Waals interactions are irrelevant, and the Hamiltonian reduces to that for a two-level system (TLS),

$$\mathcal{H}_{\rm TLS} = \Delta|s\rangle\langle s| - \Omega|g\rangle\langle s| - \Omega^*|s\rangle\langle g|. \tag{B1}$$

(We set the energy of the ground state $|g\rangle$ to zero and work in a rotating frame in which the energy of state $|e\rangle$ is also zero). The eigenstates and corresponding eigenvalues of this Hamiltonian are

$$|\pm\rangle = \frac{\varepsilon_\mp|g\rangle + \Omega|s\rangle}{\sqrt{\varepsilon_\mp^2 + |\Omega|^2}}, \quad \varepsilon_\pm = \frac{\Delta \pm \sqrt{\Delta^2 + 4|\Omega|^2}}{2}. \tag{B2}$$

For $\Delta \gg |\Omega|$, the eigenstate $|-\rangle \simeq |g\rangle + \frac{\Omega}{\Delta}|s\rangle$, with shifted energy $\varepsilon_- \simeq -\frac{|\Omega|^2}{\Delta} \equiv \delta$ (ac Stark shift), corresponds to the ground state $|g\rangle$ with a small admixture of the Rydberg state $|s\rangle$. We identify this Rydberg-dressed ground state with the spin-down state, $|\downarrow\rangle \equiv |-\rangle$, while the spin-up state is $|\uparrow\rangle \equiv |e\rangle$.

A pair of dressed ground-state atoms would interact with each other via the Rydberg state $|s\rangle$ components. Each atom is in state $|s\rangle$ with probability $\frac{|\Omega|^2}{\Delta^2}$ and therefore the two-atom interaction strength is $\frac{|\Omega|^4}{\Delta^4}V_r^{ss}$ [49]. We neglect this weak interaction and instead focus below on the interatomic interactions that are up to second order in $\frac{\Omega}{\Delta}$. Hence, with L atoms in a lattice, all in the dressed ground state, the total energy shift is

$$E_0 = \sum_i^L \delta_i = -L\frac{|\Omega|^2}{\Delta}. \tag{B3}$$

This constant energy shift can be disregarded by redefining the zero-point energy, e.g., by absorbing the ac Stark shift into the laser detuning, $\omega \to \omega + \frac{|\Omega|^2}{\Delta}$.

2. Single excitation

Assume now that one atom is excited to state $|e\rangle$ while the rest of the atoms are in the dressed ground state. Our aim is to derive the effective hopping rate of the single Rydberg excitation in the lattice and the modification of the ac Stark shifts of the ground-state atoms in the vicinity of the excited one. We are interested in the interatomic interactions that are up to second order in $\frac{\Omega}{\Delta}$, which thus involve no more than one (virtual) $|s\rangle$ excitation. It is therefore sufficient to consider the two-atom state

$$|\phi\rangle = c_{ge}|ge\rangle + c_{eg}|eg\rangle + c_{se}|se\rangle + c_{es}|es\rangle \tag{B4}$$

and the corresponding Hamiltonian

$$\begin{aligned}\mathcal{H}_{\rm at}^{(1)} = {} & \Delta_y^{(x)}|se\rangle\langle se| + \Delta_x^{(y)}|es\rangle\langle es| \\ & - \Omega(|ge\rangle\langle se| + |eg\rangle\langle es| + \text{H.c.}) \\ & + D_{xy}(|se\rangle\langle es| + \text{H.c.}),\end{aligned} \tag{B5}$$

where x and y denote the positions of the two atoms, and we defined $\Delta_y^{(x)} \equiv \Delta + V_{xy}^{se} = \Delta_x^{(y)}$. The equations for the amplitudes $c_{\nu\mu}$ of the state vector $|\phi\rangle$ are then

$$i\dot{c}_{ge} = -\Omega c_{se}, \tag{B6a}$$

$$i\dot{c}_{eg} = -\Omega c_{es}, \tag{B6b}$$

$$i\dot{c}_{se} = \left(\Delta + V_{xy}^{se}\right)c_{se} - \Omega^* c_{ge} + D_{xy}c_{es}, \tag{B6c}$$

$$i\dot{c}_{es} = \left(\Delta + V_{xy}^{se}\right)c_{es} - \Omega^* c_{eg} + D_{xy}c_{se}. \tag{B6d}$$

We adiabatically eliminate states containing the highly detuned Rydberg state $|s\rangle$. To that end, we set $\dot{c}_{se} = 0$ and $\dot{c}_{es} = 0$ and solve the last two equations for c_{se} and c_{es}. Inserting the solution into the first two equations, we obtain

$$i\dot{c}_{ge} = -\frac{|\Omega|^2\left(\Delta + V_{xy}^{se}\right)}{\left(\Delta + V_{xy}^{se}\right)^2 - D_{xy}^2}c_{ge} + \frac{|\Omega|^2 D_{xy}}{\left(\Delta + V_{xy}^{se}\right)^2 - D_{xy}^2}c_{eg}, \tag{B7a}$$

$$i\dot{c}_{eg} = -\frac{|\Omega|^2\left(\Delta + V_{xy}^{se}\right)}{\left(\Delta + V_{xy}^{se}\right)^2 - D_{xy}^2}c_{eg} + \frac{|\Omega|^2 D_{xy}}{\left(\Delta + V_{xy}^{se}\right)^2 - D_{xy}^2}c_{ge}. \tag{B7b}$$

We can interpret these equations as follows: The dressed $|g\rangle$ state atom at position y acquires an energy shift

$$\delta_y^{(x)} = -\frac{|\Omega|^2\left(\Delta + V_{xy}^{se}\right)}{\left(\Delta + V_{xy}^{se}\right)^2 - D_{xy}^2}, \tag{B8}$$

which depends on the position x of the $|e\rangle$ excitation. Besides, states $|eg\rangle$ and $|ge\rangle$ are coupled via the exchange interaction

$$J_{xy} = \frac{|\Omega|^2 D_{xy}}{\left(\Delta + V_{xy}^{se}\right)^2 - D_{xy}^2}. \tag{B9}$$

This effective excitation hopping rate $J_{xy} = J_d$ depends on the relative distance $d = |x - y|$.

Hence, the total energy of L atoms in a lattice with a single $|e\rangle$ excitation is

$$E_1 = \sum_{y\neq x} \delta_y^{(x)}. \tag{B10}$$

This sum has now $L - 1$ terms. The terms $\delta_y^{(x)}$ with small separation $|x - y| \geqslant 1$ are affected by the D_{xy} and V_{xy}^{se} interactions, while the terms with $|x - y| \gg 1$ are obviously equal to the ac Stark shift $\delta = -\frac{|\Omega|^2}{\Delta}$ of a noninteracting atom. Due to the translational invariance of the lattice, E_1 does not depend on the position x of the $|e\rangle$ excitation. E_1 is therefore a constant which can be disregarded by redefining the zero-point energy (notice, however, that $E_1 \neq E_0$).

We thus obtain an effective Hamiltonian for a single excitation hopping on a lattice,

$$\begin{aligned}\mathcal{H}_J^{(1)} &= \sum_{x\neq y} J_{xy}|x\rangle\langle y| \\ &= \sum_{x=1}^{L}\sum_{d\geqslant 1} J_d(|x\rangle\langle x+d| + |x\rangle\langle x-d|),\end{aligned} \tag{B11}$$

which has the same form as $\mathcal{H}_J^{(1)}$ in the main text. For $\Delta \gg D_d, V_d^{es}$, the excitation hopping rates

$$J_d \simeq \frac{|\Omega|^2 D_d}{\Delta^2} \propto 1/d^3 \tag{B12}$$

can be truncated to range $d_J = 2$.

3. Two excitations

Consider finally two $|e\rangle$ excitations in the lattice. As argued above, to determine interatomic interactions that are up to second order in $\frac{\Omega}{\Delta}$, we can restrict our analysis to the multiatom configurations with at most one atom in state $|s\rangle$. It is then sufficient to consider the three-atom state

$$\begin{aligned}|\phi\rangle = {} & c_{gee}|gee\rangle + c_{ege}|ege\rangle + c_{eeg}|eeg\rangle \\ & + c_{see}|see\rangle + c_{ese}|ese\rangle + c_{ees}|ees\rangle.\end{aligned} \tag{B13}$$

We assume, as before, that the interaction V_d^{ee} between the $|e\rangle$ excitations is weak, $V_d^{ee} \ll \Omega, D_d \ll \Delta$, and neglect it here; later we account for V_d^{ee} exactly in the effective Hamiltonian. The three-atom Hamiltonian is

$$\begin{aligned}\mathcal{H}_{\rm at}^{(2)} = {} & \Delta_{x,y}^{(z)}|ees\rangle\langle ees| + \Delta_{x,z}^{(y)}|ese\rangle\langle ese| + \Delta_{y,z}^{(x)}|see\rangle\langle see| \\ & - \Omega(|gee\rangle\langle see| + |ege\rangle\langle ese| + |eeg\rangle\langle ees| + \text{H.c.}) \\ & + D_{xy}(|see\rangle\langle ese| + \text{H.c.}) \\ & + D_{xz}(|see\rangle\langle ees| + \text{H.c.}) \\ & + D_{yz}(|ese\rangle\langle ees| + \text{H.c.}),\end{aligned} \tag{B14}$$

where x, y, z denote the positions of the atoms, $\Delta_{x,y}^{(z)} \equiv \Delta + V_{xz}^{se} + V_{yz}^{se}$, and similarly for $\Delta_{x,z}^{(y)}$ and $\Delta_{y,z}^{(x)}$. From the differential equations for the amplitudes $c_{\lambda\mu\nu}$ of $|\phi\rangle$, we adiabatically eliminate the amplitudes corresponding to the highly detuned $|s\rangle$ state, i.e., we set $\dot{c}_{ees} = \dot{c}_{ese} = \dot{c}_{see} = 0$, solve for the amplitudes $c_{ees}, c_{ese}, c_{see}$, and insert them into the remaining equations. The resulting equations have the form

$$\begin{aligned}\dot{c}_{eeg} = {} & \frac{|\Omega|^2\left(\Delta_{x,z}^{(y)}\Delta_{y,z}^{(x)} - D_{xy}^2\right)}{\Gamma(x,y,z)}c_{eeg} \\ & + \frac{|\Omega|^2\left(D_{xy}D_{xz} - D_{yz}\Delta_{y,z}^{(x)}\right)}{\Gamma(x,y,z)}c_{ege} \\ & + \frac{|\Omega|^2\left(D_{xy}D_{yz} - D_{xz}\Delta_{x,z}^{(y)}\right)}{\Gamma(x,y,z)}c_{gee},\end{aligned} \tag{B15}$$

with $\Gamma(x,y,z) \equiv -\Delta_{x,y}^{(z)}\Delta_{x,z}^{(y)}\Delta_{y,z}^{(x)} - 2D_{xy}D_{xz}D_{yz} + \Delta_{x,y}^{(z)}D_{xy}^2 + \Delta_{x,z}^{(y)}D_{xz}^2 + \Delta_{y,z}^{(x)}D_{yz}^2$, and similarly for $\dot{c}_{ege}$ and $\dot{c}_{gee}$. The first term in Eq. (B15) corresponds to the energy shift of the dressed $|g\rangle$ state atom, while the other two terms describe the exchange interactions between the atom in state $|g\rangle$ and the atoms in state $|e\rangle$.

Using series expansion in $\frac{\Omega}{\Delta} \ll 1$, the energy shift of the ground-state atom at position z can be cast as

$$\begin{aligned}\delta_z^{(x,y)} = {} & -\frac{|\Omega|^2}{\Delta_{x,y}^{(z)}} - \frac{|\Omega|^2 D_{xz}^2}{\left(\Delta_{x,y}^{(z)}\right)^2\Delta_{z,y}^{(x)}} \\ & - \frac{|\Omega|^2 D_{yz}^2}{\left(\Delta_{x,y}^{(z)}\right)^2\Delta_{x,z}^{(y)}} + O\left(\frac{|\Omega|^4}{\Delta^4}\right).\end{aligned} \tag{B16}$$

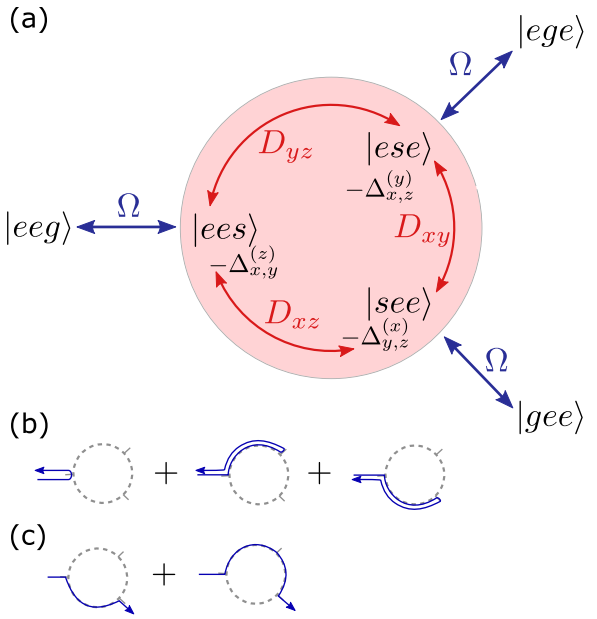

FIG. 5. (a) Diagram of transitions for retrieving the perturbative energy shifts and excitation hopping rates for two excited $|e\rangle$ and one ground $|g\rangle$ state atoms. The atomic positions are x,y,z. The red shaded region denotes the high-energy subspace, $\Delta \gg \Omega, D$, which is eliminated adiabatically. (b) Illustration of three virtual processes contributing to the energy shift of $|eeg\rangle$, as per Eq. (B16). (c) Two possible paths for the hopping process $|eeg\rangle \leftrightarrow |gee\rangle$ given by Eq. (B17).

Here, the first term is the second-order ac Stark shift of the $|g\rangle$ state atom due to virtual excitation to state $|s\rangle$ via the nonresonant laser field. The next two terms describe higher-order shifts due to the laser excitation followed by exchange interaction with the $|e\rangle$ state atoms. Similarly, we can cast the excitation hopping $|eeg\rangle \leftrightarrow |gee\rangle$ between the atoms at positions x and z as

$$J^{(y)}_{xz} = \frac{|\Omega|^2 D_{xz}}{\Delta^z_{x,y}\Delta^x_{z,y}} - \frac{|\Omega|^2 D_{yz} D_{xy}}{\Delta^z_{x,y}\Delta^x_{y,z}\Delta^y_{z,x}} + O\left(\frac{|\Omega|^4}{\Delta^4}\right). \quad \text{(B17)}$$

Here, the first term describes the laser-mediated excitation hopping via direct dipole-dipole exchange interaction between the atoms at positions x and z. The second term describes the excitation hopping via indirect process that involves, first, exchange interaction between the $|e\rangle$ state atom at position y and the virtually $|s\rangle$ excited atom at z, followed by exchange interaction between the $|s\rangle$ state atom now at y and the $|e\rangle$ state atom at position x. Analogously, we obtain the hopping rates for $|eeg\rangle \leftrightarrow |ege\rangle$ and $|ege\rangle \leftrightarrow |gee\rangle$. In Fig. 5 we illustrate the virtual processes that lead the perturbative energy shifts and excitation hoppings.

The effective low-energy Hamiltonian for two excited-state atoms and one ground-state atom can now be cast as

$$\begin{aligned}\mathcal{H}^{(2)}_{\rm eff} = {} & \left(\delta^{(y,z)}_x + V^{ee}_{yz}\right)|gee\rangle\langle gee| + \left(\delta^{(x,z)}_y + V^{ee}_{xz}\right)|ege\rangle\langle ege| \\ & + \left(\delta^{(x,y)}_z + V^{ee}_{xy}\right)|eeg\rangle\langle eeg| + J^{(z)}_{xy}(|gee\rangle\langle ege| + \text{H.c.}) \\ & + J^{(y)}_{xz}(|eeg\rangle\langle gee| + \text{H.c.}) + J^{(x)}_{yz}(|ege\rangle\langle eeg| + \text{H.c.}),\end{aligned} \quad \text{(B18)}$$

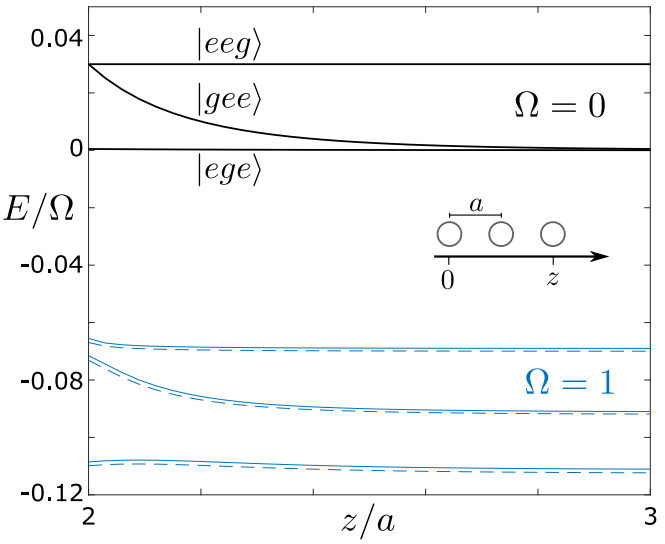

FIG. 6. Comparison of the low-energy spectra of the exact Hamiltonian (B14) including the interactions V^{ee}_r (solid lines), and the effective Hamiltonian (B18) (dashed lines). The positions of the first and second atoms are fixed, $x = 0$ and $y = a$, while the position of the third atom varies: $z \geqslant 2a$. Black lines at $E \geqslant 0$ show the exact spectrum for $\Omega = 0$, corresponding to the bare states $|ege\rangle$, $|gee\rangle$, and $|eeg\rangle$. Blue lines show the spectra for the dressed states with the parameters $\Delta/\Omega = 10$, $D_1/\Omega = 1$, $V^{se}_1/\Omega = -1/8$, and $V^{ee}_1/\Omega = 0.03$ ($D_r \propto 1/r^3$, $V_r \propto 1/r^6$).

where we have included the interactions V^{ee}_r between the $|e\rangle$ state atoms. In Fig. 6 we show the spectrum of this Hamiltonian for varying the position z of the third atom, while the first and second atoms are at positions $x = 0$ and $y = a$. For comparison, we also show the low-energy part of the spectrum of the exact Hamiltonian (B14) including also the interactions V^{ee}_r. We observe that the effective Hamiltonian reproduces very well the low-energy part of the exact Hamiltonian. Clearly, the discrepancy between the exact and effective models decreases by increasing the detuning Δ, and in the limit of $\Omega/\Delta \to 0$ the effective model reduces to the low-energy part of the exact model.

Effective lattice Hamiltonian

We can now extend the three-atom model to a system of L atoms on a lattice (setting the lattice constant $a = 1$). We start with the transport term of the Hamiltonian. Denoting by x and y the positions of the two excitations and using the notation $J^{(y)}_{xz} \equiv J_d(r)$ with $d \equiv |x - z|$ and $r = |x - y|$, we have

$$\begin{aligned}\mathcal{H}^{(2)}_J = \sum_{x<y}\Bigg[& \sum_d J_d(r)(|x,y\rangle\langle x-d,y| + |x,y\rangle\langle x,y+d|) \\ & + \sum_{d<y-x} J_d(r)(|x,y\rangle\langle x+d,y| + |x,y\rangle\langle x,y-d|) \\ & + \sum_{d>y-x} J_d(r)(|x,y\rangle\langle y,x+d| + |x,y\rangle\langle y-d,x|)\Bigg],\end{aligned} \quad \text{(B19)}$$

which has the same form as Eq. (4) but with the hopping rates $J_d(r)$ that depend on the relative distance r between the two

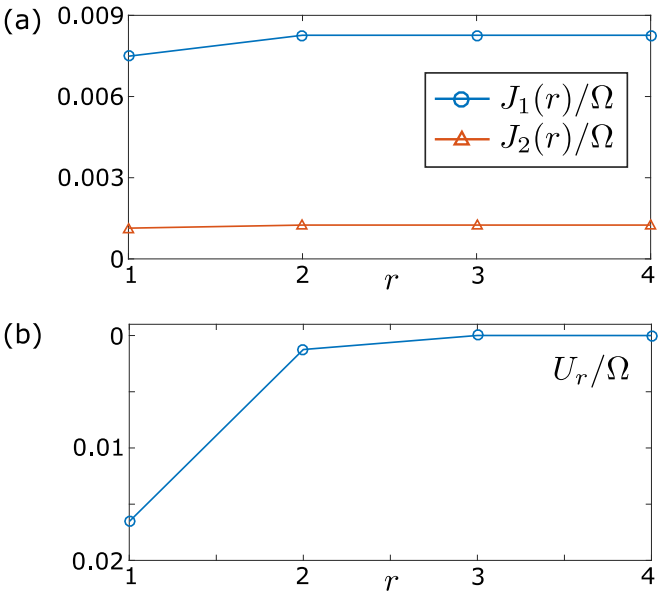

FIG. 7. (a) One- and two-site hopping rates $J_1(r)$ and $J_2(r)$ versus distance r between the two excitations. (b) Interaction potential U_r of Eq. (B23), for $V_1^{ee}=0$. The parameters are $\Delta/\Omega=10$, $D_1/\Omega=1$, and $V_1^{se}/\Omega=1$.

excitations. Since in the leading order $J_d(r)\propto D_d\sim 1/d^3$, we truncate it to range $d_J=2$. As in the main text, we can transform $\mathcal{H}_J^{(2)}$ to the center of mass R and relative r coordinates and diagonalize the center-of-mass part by Fourier transform $|R\rangle=\frac{1}{\sqrt{L}}\sum_K e^{iKR}|K\rangle$, obtaining

$$\begin{aligned}\mathcal{H}_J^{(2)}=&\sum_K |K\rangle\langle K|\\ &\otimes\Big\{\sum_{r\geqslant 1}[2J_1(r)\cos(K/2)|r\rangle\langle r+1|+|r+1\rangle\langle r|)\\ &+2J_2(r)\cos(K)(|r\rangle\langle r+2|+|r+2\rangle\langle r|)]\\ &+2J_2'(1)\cos(K)|1\rangle\langle 1|\Big\}.\end{aligned}\tag{B20}$$

From Eq. (B17) we have for the hopping rates

$$J_1(r=1)=\frac{|\Omega|^2D_1}{(\Delta+V_1^{se})(\Delta+2V_1^{se})}\left(1-\frac{D_2}{\Delta+V_1^{se}}\right),\tag{B21a}$$

$$J_1(r\geqslant 2)=\frac{|\Omega|^2D_1}{(\Delta+V_1^{se})^2},\tag{B21b}$$

$$J_2(r=1)=\frac{|\Omega|^2D_2}{\Delta(\Delta+V_1^{se})},\tag{B21c}$$

$$J_2(r\geqslant 2)=\frac{|\Omega|^2D_2}{\Delta^2},\tag{B21d}$$

$$J_2'(1)=\frac{|\Omega|^2D_2}{(\Delta+V_1^{se})^2}\left(1-\frac{D_1^2/D_2}{\Delta+2V_1^{se}}\right),\tag{B21e}$$

where we set $V_{d\geqslant 2}^{se}=0$ and $D_{d\geqslant 3}=0$. In Fig. 7(a) we show the dependence of the one- and two-site hopping rates on the relative distance r between the excitations. While $J_2(r)$ is nearly constant for the relevant parameter regime, $J_1(r)$ has a noticeable dip at $r=1$ for large $V_1^{se}\sim\Omega$. It follows from Eq. (B21a) that $J_1(r)$ becomes r independent for $V_1^{se}=-D_2$. Since we assumed that $D_d=\frac{C_3/a^3}{d^3}$ and $V_d^{se}=\frac{C_6^{se}/a^6}{d^6}$, the required lattice constant is $a=2\sqrt[3]{-C_6^{se}/C_3}$ with the interaction coefficients C_6^{se} and C_3 having opposite sign. Notice that $J_2'(1)$ in Eq. (B21e), responsible for the two-excitation "somersault," can be tuned by Δ or even made to vanish. Thus $J_2'(1)=0$ for $\Delta+2V_1^{se}=D_1^2/D_2$, which, with $D_2=D_1/8$ and $V_1^{se}\ll\Delta$, requires $\Delta\simeq 8D_1$.

For $\Delta\gg\Omega, D_1\gg D_2, V_1^{es}$, the excitation hopping rates of Eqs. (B21) can be well approximated by r-independent rates J_d of Eq. (11) in the main text.

Consider next the effective interaction between the excitations. The total energy of L atoms in a lattice with two $|e\rangle$ excitations is

$$E_2(x,y)=\sum_{z\neq x,y}\delta_z^{(x,y)}.\tag{B22}$$

This sum has now $L-2$ terms and it depends on the positions x and y of the two excitations as per Eq. (B16). Due to translational invariance of the lattice, $E_2(r)$ depends only on the relative distance $r=|x-y|$. For large r, $E_2(r)$ tends to a constant since each dressed ground-state atom can have at most one excited atom in its vicinity. Setting $E_2(r\to\infty)$ as the zero point energy, we can then define the interaction potential between the two excitations as

$$U_r=E_2(r)-E_2(r\to\infty).\tag{B23}$$

Setting, as before, $V_{d\geqslant 2}^{se}=0$ and $D_{d\geqslant 3}=0$, we obtain an effective interaction potential U_r having range $d_U=3$,

$$\begin{aligned}U_1=&V_1^{ee}-2\left(\frac{|\Omega|^2}{\Delta}-\frac{|\Omega|^2}{\Delta+V_1^{se}}\right)\\ &+2\frac{|\Omega|^2D_1^2}{(\Delta+V_1^{se})^2}\left(\frac{2}{\Delta+V_1^{se}}-\frac{1}{\Delta+2V_1^{se}}\right)\\ &+2|\Omega|^2D_2^2\left(\frac{2}{\Delta^3}-\frac{1}{\Delta^2(\Delta+V_1^{se})}-\frac{1}{(\Delta+V_1^{se})^3}\right),\end{aligned}\tag{B24a}$$

$$\begin{aligned}U_2=&V_2^{ee}-\left(\frac{|\Omega|^2}{\Delta}-\frac{|\Omega|^2}{\Delta+V_1^{se}}\right)\\ &+2\frac{|\Omega|^2D_1^2}{\Delta+V_1^{se}}\left(\frac{1}{(\Delta+V_1^{se})^2}-\frac{1}{(\Delta+2V_1^{se})^2}\right)\\ &+2\frac{|\Omega|^2D_2^2}{\Delta^3},\end{aligned}\tag{B24b}$$

$$U_3=V_3^{ee}+2\frac{|\Omega|^2D_2^2}{\Delta}\left(\frac{1}{\Delta^2}-\frac{1}{(\Delta+V_1^{se})^2}\right),\tag{B24c}$$

where for consistency we included the interactions V_r^{ee} up to range $d_U=3$. In Fig. 7(b) we show the interaction potential U_r of Eq. (B23), i.e., Eqs. (B24) without V_r^{ee}. Clearly, the nearest-neighbor interaction U_1 is stronger than $U_{r\geqslant 2}$. Thus, neglecting $U_{r\geqslant 2}$ would correspond to the spin-lattice model

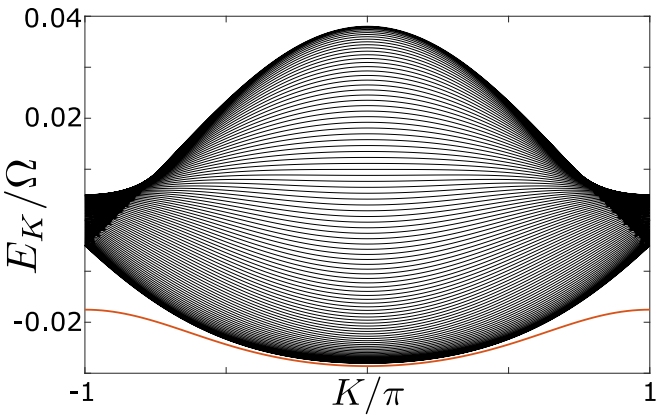

FIG. 8. Scattering and bound spectrum for two $|e\rangle$ excitations in a lattice, with the parameters as in Fig. 7.

studied in the text. We can now write the interaction term of the Hamiltonian as

$$\mathcal{H}_U^{(2)} = \sum_K |K\rangle\langle K| \otimes \sum_{r=1}^{3} U_r |r\rangle\langle r|, \tag{B25}$$

which has the same form as Eq. (A3).

To summarize, the total Hamiltonian for two $|e\rangle$ excitations in a lattice of Rydberg dressed atoms is

$$\mathcal{H}^{(2)} = \mathcal{H}_J^{(2)} + \mathcal{H}_U^{(2)}, \tag{B26}$$

where $\mathcal{H}_J^{(2)}$ and $\mathcal{H}_U^{(2)}$ are given by Eqs. (B20) and (B25), respectively. In Fig. 1(a) of the main text we show the spectrum of this Hamiltonian. The scattering states are insensitive to the variations of $J_d(r)$ and U_r at short range, $r \leqslant 3$, so the scattering spectrum is well reproduced by the spin-lattice model Hamiltonian with r-independent hopping rates J_d and only the nearest-neighbor interaction U_1. The spin-lattice model approximates well also the bound states of Hamiltonian (B26), especially for U_r dominated by the nearest-neighbor interatomic interaction V_1^{ee} and constant J_1 achieved for $V_1^{se} = -D_2$, which is used in Fig. 1(a).

Note that even without interatomic interactions, $V_r^{ee}, V_r^{se} = 0$, we still have nonvanishing effective interaction $U_1 \simeq 2\frac{|\Omega|^2 D_1^2}{\Delta^3}$, which is, however, too weak compared to $J_1 \simeq \frac{|\Omega|^2 D_1}{\Delta^2}$ to sustain a bound state (see the lower panel of Fig. 3). But strong enough interatomic interaction $|V_1^{se}| \simeq \Omega, D_1 \ll \Delta$ resulting in $U_1 \simeq -2\frac{|\Omega|^2 V_1^{se}}{\Delta^2}$ can sustain a two-excitation bound state, as shown in Fig. 8. The corresponding hopping rate $J_1(r)$ has now sizable r dependence (see Fig. 7).

[1] R. P. Feynman, Simulating physics with computers, Int. J. Theor. Phys. **21**, 467 (1982).

[2] S. Lloyd, Universal quantum simulators, Science **273**, 1073 (1996).

[3] R. Blatt and C. F. Roos, Quantum simulations with trapped ions, Nat. Phys. **8**, 277 (2012).

[4] J. Zhang, G. Pagano, P. W. Hess, A. Kyprianidis, P. Becker, H. Kaplan, A. V. Gorshkov, Z.-X. Gong, and C. Monroe, Observation of a many-body dynamical phase transition with a 53-qubit quantum simulator, Nature (London) **551**, 601 (2017).

[5] A. A. Houck, H. E. Türeci, and J. Koch, On-chip quantum simulation with superconducting circuits, Nat. Phys. **8**, 292 (2012).

[6] C. Neill, P. Roushan, K. Kechedzhi, S. Boixo, S. V. Isakov, V. Smelyanskiy, R. Barends, B. Burkett, Y. Chen, Z. Chen, B. Chiaro, A. Dunsworth, A. Fowler, B. Foxen, R. Graff, E. Jeffrey, J. Kelly, E. Lucero, A. Megrant, J. Mutus, M. Neeley, C. Quintana, D. Sank, A. Vainsencher, J. Wenner, T. C. White, H. Neven, and J. M. Martinis, A blueprint for demonstrating quantum supremacy with superconducting qubits, arXiv:1709.06678.

[7] T. Hensgens, T. Fujita, L. Janssen, X. Li, C. J. Van Diepen, C. Reichl, W. Wegscheider, S. D. Sarma, and L. M. K. Vandersypen, Quantum simulation of a Fermi-Hubbard model using a semiconductor quantum dot array, Nature (London) **548**, 70 (2017).

[8] C. Gross and I. Bloch, Quantum simulations with ultracold atoms in optical lattices, Science **357**, 995 (2017).

[9] A. B. Kuklov and B. V. Svistunov, Counterflow Superfluidity of Two-Species Ultracold Atoms in a Commensurate Optical Lattice, Phys. Rev. Lett. **90**, 100401 (2003).

[10] L.-M. Duan, E. Demler, and M. D. Lukin, Controlling Spin Exchange Interactions of Ultracold Atoms in Optical Lattices, Phys. Rev. Lett. **91**, 090402 (2003).

[11] S. Trotzky, P. Cheinet, S. Fölling, M. Feld, U. Schnorrberger, A. M. Rey, A. Polkovnikov, E. A. Demler, M. D. Lukin, and I. Bloch, Time-resolved observation and control of superexchange interactions with ultracold atoms in optical lattices, Science **319**, 295 (2008).

[12] Y.-A. Chen, S. Nascimbène, M. Aidelsburger, M. Atala, S. Trotzky, and I. Bloch, Controlling Correlated Tunneling and Superexchange Interactions with ac-Driven Optical Lattices, Phys. Rev. Lett. **107**, 210405 (2011).

[13] T. Lahaye, C. Menotti, L. Santos, M. Lewenstein, and T. Pfau, The physics of dipolar bosonic quantum gases, Rep. Prog. Phys. **72**, 126401 (2009).

[14] S. A. Moses, J. P. Covey, M. T. Miecnikowski, D. S. Jin, and J. Ye, New frontiers for quantum gases of polar molecules, Nat. Phys. **13**, 13 (2017).

[15] D. Greif, T. Uehlinger, G. Jotzu, L. Tarruell, and T. Esslinger, Short-range quantum magnetism of ultracold fermions in an optical lattice, Science **340**, 1307 (2013).

[16] M. Boll, T. A. Hilker, G. Salomon, A. Omran, J. Nespolo, L. Pollet, I. Bloch, and C. Gross, Spin- and density-resolved microscopy of antiferromagnetic correlations in Fermi-Hubbard chains, Science **353**, 1257 (2016).

[17] A. Mazurenko, C. S. Chiu, G. Ji, M. F. Parsons, M. Kanasz-Nagy, R. Schmidt, F. Grusdt, E. Demler, D. Greif, and M. Greiner, A cold-atom Fermi Hubbard antiferromagnet, Nature (London) **545**, 462 (2017).

[18] D. Barredo, S. de Léséleuc, V. Lienhard, T. Lahaye, and A. Browaeys, An atom-by-atom assembler of defect-free arbitrary two-dimensional atomic arrays, Science **354**, 1021 (2016).

[19] M. Endres, H. Bernien, A. Keesling, H. Levine, E. R. Anschuetz, A. Krajenbrink, C. Senko, V. Vuletic, M. Greiner, and M. D. Lukin, Atom-by-atom assembly of defect-

free one-dimensional cold atom arrays, Science **354**, 1024 (2016).
[20] I. Bouchoule and K. Mølmer, Spin squeezing of atoms by the dipole interaction in virtually excited Rydberg states, Phys. Rev. A **65**, 041803 (2002).
[21] J. E. Johnson and S. L. Rolston, Interactions between Rydberg-dressed atoms, Phys. Rev. A **82**, 033412 (2010).
[22] T. Macrì and T. Pohl, Rydberg dressing of atoms in optical lattices, Phys. Rev. A **89**, 011402 (2014).
[23] Y.-Y. Jau, A. M. Hankin, T. Keating, I. H. Deutsch, and G. W. Biedermann, Entangling atomic spins with a Rydberg-dressed spin-flip blockade, Nat. Phys. **12**, 71 (2016).
[24] P. Schauß, M. Cheneau, M. Endres, T. Fukuhara, S. Hild, A. Omran, T. Pohl, C. Gross, S. Kuhr, and I. Bloch, Observation of spatially ordered structures in a two-dimensional Rydberg gas, Nature (London) **491**, 87 (2012).
[25] P. Schauß, J. Zeiher, T. Fukuhara, S. Hild, M. Cheneau, T. Macrì, T. Pohl, I. Bloch, and C. Gross, Crystallization in Ising quantum magnets, Science **347**, 1455 (2015).
[26] H. Labuhn, D. Barredo, S. Ravets, S. de Léséleuc, T. Macri, T. Lahaye, and A. Browaeys, Tunable two-dimensional arrays of single Rydberg atoms for realizing quantum Ising models, Nature (London) **534**, 667 (2016).
[27] V. Lienhard, S. de Léséleuc, D. Barredo, T. Lahaye, A. Browaeys, M. Schuler, L.-P. Henry, and A. M. Läuchli, Observing the space- and time-dependent growth of correlations in dynamically tuned synthetic Ising antiferromagnets, arXiv:1711.01185.
[28] H. Bernien, S. Schwartz, A. Keesling, H. Levine, A. Omran, H. Pichler, S. Choi, A. S. Zibrov, M. Endres, M. Greiner, V. Vuletic, and M. D. Lukin, Probing many-body dynamics on a 51-atom quantum simulator, Nature (London) **551**, 579 (2017).
[29] T. Fukuhara, P. Schauß, M. Endres, S. Hild, M. Cheneau, I. Bloch, and C. Gross, Microscopic observation of magnon bound states and their dynamics, Nature (London) **502**, 76 (2013).
[30] K. Winkler, G. Thalhammer, F. Lang, R. Grimm, J. H. Denschlag, A. J. Daley, A. Kantian, H. P. Büchler, and P. Zoller, Repulsively bound atom pairs in an optical lattice, Nature (London) **441**, 853 (2006).
[31] R. Piil and K. Mølmer, Tunneling couplings in discrete lattices, single-particle band structure, and eigenstates of interacting atom pairs, Phys. Rev. A **76**, 023607 (2007).
[32] D. Petrosyan, B. Schmidt, J. R. Anglin, and M. Fleischhauer, Quantum liquid of repulsively bound pairs of particles in a lattice, Phys. Rev. A **76**, 033606 (2007).
[33] M. Valiente and D. Petrosyan, Two-particle states in the Hubbard model, J. Phys. B **41**, 161002 (2008).
[34] M. Valiente and D. Petrosyan, Scattering resonances and two-particle bound states of the extended Hubbard model, J. Phys. B **42**, 121001 (2009).
[35] M. Valiente, Lattice two-body problem with arbitrary finite-range interactions, Phys. Rev. A **81**, 042102 (2010).
[36] J. Javanainen, O. Odong, and J. C. Sanders, Dimer of two bosons in a one-dimensional optical lattice, Phys. Rev. A **81**, 043609 (2010).
[37] J. Sous, M. Berciu, and R. V. Krems, Bipolarons bound by repulsive phonon-mediated interactions, Phys. Rev. A **96**, 063619 (2017).
[38] R. Côté, A. Russell, E. E. Eyler, and P. L. Gould, Quantum random walk with Rydberg atoms in an optical lattice, New J. Phys. **8**, 156 (2006).
[39] D. Barredo, H. Labuhn, S. Ravets, T. Lahaye, A. Browaeys, and C. S. Adams, Coherent Excitation Transfer in a Spin Chain of Three Rydberg Atoms, Phys. Rev. Lett. **114**, 113002 (2015).
[40] S. de Léséleuc, D. Barredo, V. Lienhard, A. Browaeys, and T. Lahaye, Optical Control of the Resonant Dipole-Dipole Interaction between Rydberg Atoms, Phys. Rev. Lett. **119**, 053202 (2017).
[41] M. Saffman, T. G. Walker, and K. Mølmer, Quantum information with Rydberg atoms, Rev. Mod. Phys. **82**, 2313 (2010).
[42] B. Vermersch, A. W. Glaetzle, and P. Zoller, Magic distances in the blockade mechanism of Rydberg p and d states, Phys. Rev. A **91**, 023411 (2015).
[43] N. Henkel, R. Nath, and T. Pohl, Three-Dimensional Roton Excitations and Supersolid Formation in Rydberg-Excited Bose-Einstein Condensates, Phys. Rev. Lett. **104**, 195302 (2010).
[44] G. Pupillo, A. Micheli, M. Boninsegni, I. Lesanovsky, and P. Zoller, Strongly Correlated Gases of Rydberg-Dressed Atoms: Quantum and Classical Dynamics, Phys. Rev. Lett. **104**, 223002 (2010).
[45] S. Wüster, C. Ates, A. Eisfeld, and J. M. Rost, Excitation transport through Rydberg dressing, New J. Phys. **13**, 073044 (2011).
[46] H. Schempp, G. Günter, S. Wüster, M. Weidemüller, and S. Whitlock, Correlated Exciton Transport in Rydberg-Dressed-Atom Spin Chains, Phys. Rev. Lett. **115**, 093002 (2015).
[47] A. W. Glaetzle, M. Dalmonte, R. Nath, C. Gross, I. Bloch, and P. Zoller, Designing Frustrated Quantum Magnets with Laser-Dressed Rydberg Atoms, Phys. Rev. Lett. **114**, 173002 (2015).
[48] R. M. W. van Bijnen and T. Pohl, Quantum Magnetism and Topological Ordering via Rydberg Dressing near Förster Resonances, Phys. Rev. Lett. **114**, 243002 (2015).
[49] L. F. Buchmann, K. Mølmer, and D. Petrosyan, Creation and transfer of nonclassical states of motion using Rydberg dressing of atoms in a lattice, Phys. Rev. A **95**, 013403 (2017).
[50] J. Zeiher, R. van Bijnen, P. Schauß, S. Hild, J.-Y. Choi, T. Pohl, I. Bloch, and C. Gross, Many-body interferometry of a Rydberg-dressed spin lattice, Nat. Phys. **12**, 1095 (2016).
[51] J. Zeiher, J.-yoon Choi, A. Rubio-Abadal, T. Pohl, R. van Bijnen, I. Bloch, and C. Gross, Coherent Many-Body Spin Dynamics in a Long-Range Interacting Ising Chain, Phys. Rev. X **7**, 041063 (2017).
[52] L. Béguin, A. Vernier, R. Chicireanu, T. Lahaye, and A. Browaeys, Direct Measurement of the van der Waals Interaction between Two Rydberg Atoms, Phys. Rev. Lett. **110**, 263201 (2013).
[53] A. Browaeys, D. Barredo, and T. Lahaye, Experimental investigations of dipole-dipole interactions between a few Rydberg atoms, J. Phys. B **49**, 152001 (2016).
[54] I. I. Beterov, I. I. Ryabtsev, D. B. Tretyakov, and V. M. Entin, Quasiclassical calculations of blackbody-radiation-induced depopulation rates and effective lifetimes of Rydberg ns, np, and nd alkali-metal atoms with $n \leqslant 80$, Phys. Rev. A **79**, 052504 (2009).
[55] E. A. Goldschmidt, T. Boulier, R. C. Brown, S. B. Koller, J. T. Young, A. V. Gorshkov, S. L. Rolston, and J. V. Porto, Anomalous Broadening in Driven Dissipative Rydberg Systems, Phys. Rev. Lett. **116**, 113001 (2016).

[56] T. Boulier, E. Magnan, C. Bracamontes, J. Maslek, E. A. Goldschmidt, J. T. Young, A. V. Gorshkov, S. L. Rolston, and J. V. Porto, Spontaneous avalanche dephasing in large Rydberg ensembles, Phys. Rev. A **96**, 053409 (2017).

[57] J. T. Young, T. Boulier, E. Magnan, E. A. Goldschmidt, R. M. Wilson, S. L. Rolston, J. V. Porto, and A. V. Gorshkov, Dissipation-induced dipole blockade and antiblockade in driven Rydberg systems, Phys. Rev. A **97**, 023424 (2018).

[58] M. Saffman, Quantum computing with atomic qubits and Rydberg interactions: Progress and challenges, J. Phys. B **49**, 202001 (2016).

[59] W. Li, C. Ates, and I. Lesanovsky, Nonadiabatic Motional Effects and Dissipative Blockade for Rydberg Atoms Excited from Optical Lattices or Microtraps, Phys. Rev. Lett. **110**, 213005 (2013).

[60] S. Zhang, F. Robicheaux, and M. Saffman, Magic-wavelength optical traps for Rydberg atoms, Phys. Rev. A **84**, 043408 (2011).

[61] M. Mattioli, M. Dalmonte, W. Lechner, and G. Pupillo, Cluster Luttinger Liquids of Rydberg-Dressed Atoms in Optical Lattices, Phys. Rev. Lett. **111**, 165302 (2013).

[62] M. Dalmonte, W. Lechner, Z. Cai, M. Mattioli, A. M. Läuchli, and G. Pupillo, Cluster Luttinger liquids and emergent supersymmetric conformal critical points in the one-dimensional soft-shoulder Hubbard model, Phys. Rev. B **92**, 045106 (2015).

[63] D. W. Schönleber, A. Eisfeld, M. Genkin, S. Whitlock, and S. Wüster, Quantum Simulation of Energy Transport with Embedded Rydberg Aggregates, Phys. Rev. Lett. **114**, 123005 (2015).